Available online at www.sciencedirect.com
SCIENCE DIRECT®
Journal of Power Sources 128 (2004) 13–24
JOURNAL OF POWER SOURCES
www.elsevier.com/locate/jpowsour

Cold start simulations of a gasoline based fuel processor for mobile fuel cell applications

S. Springmann [a,*], M. Bohnet [b], A. Docter [c], A. Lamm [d], G. Eigenberger [b]

[a] *Rosenbergstr. 91, 70193 Stuttgart, Germany*
[b] *Institut für Chemische Verfahrenstechnik, Böblingerstr. 72, 70199 Stuttgart, Germany*
[c] *DaimlerChrysler AG, 096/G252-RBP, 70546 Stuttgart, Germany*
[d] *DaimlerChrysler AG, EP/FAF, HPCC X773, 71059 Sindelfingen, Germany*

Received 29 April 2003; received in revised form 4 September 2003; accepted 8 September 2003

Abstract

The cold start behaviour of the gas processing unit is one crucial issue for the use of gasoline based fuel reformers for mobile fuel cell systems. In this contribution different cold start strategies for a mobile fuel reformer based on gasoline are presented and discussed. The simulation studies are based on 1-d, dynamic multiphase models for both an autothermal gasoline reformer (ATR) and a thermally integrated reforming unit consisting of an ATR, a heat exchanger and a high-temperature-shift-reactor (HTS). Setup and geometric parameters for both models correspond to pilot stage systems considered by DaimlerChrysler.

Results on the reactive heat-up of the ATR by partial and total oxidation of gasoline show the impact of the air/fuel-ratio and the thermal load on the cold start duration. The use of the reformat during the rapid start-up of the ATR is mainly limited by the availability of steam for autothermal operation. Due to the high thermal capacities of the system, the whole reforming unit requires much longer time for the cold start. Especially the slow convective heat-up of the HTS restricts the conversion of CO and the subsequent use of the reformat in the fuel cell. Several options for the acceleration of the cold start were investigated. Both a simple λ-control strategy and the reactive heat-up of the HTS by (partial) oxidation of the reformat with injected air reduce the cold start time significantly. With these measures a hydrogen-rich reformat with acceptable CO-concentration is available within two minutes. Moreover, the cold start time can be further reduced, if the HTS is heated up electrically to their ignition temperature at the beginning of the cold start. Thereby the CO-conversion in the HTS already starts in the first minute and, depending on the availability of steam for the feed stream, a cold start of the reforming unit below one minute seems to be possible.

Keywords: Fuel cell; Dynamic simulation; Cold start; Gasoline

1. Fundamentals and modelling

The use of fuel cells for mobile applications in an auxiliary power unit or a propulsion system has been widely discussed and already announced by several car manufacturers. While the majority in automobile and oil industry accounts hydrogen as the ideal long-term fuel for mobile fuel cell systems, it is not yet clear, what will be the best fuel for the introduction of these systems [1]. The use of hydrogen results in high efficiencies and a simple system design. Liquid fuels like methanol or gasoline on the other hand show advantages in terms of high energy density, easy fuel handling and—in the case of gasoline—in an existing fuel infrastructure. Therefore, all major car manufacturers are developing both hydrogen and gasoline based fuel cell systems. Since gasoline must be converted into a hydrogen-rich gas (reformat) onboard, such systems have to be much more elaborate than the hydrogen based systems. Besides of the fuel cell, a gasoline based system typically consists of an autothermal reformer (ATR), where gasoline in converted into a hydrogen-rich gas, and of several subsequent gas-cleaning stages, like watergas-shift-reactors and selective oxidation-reactors [2–5]. These are necessary for the removal of CO, which is a strong poison for the fuel cell catalyst. Fig. 1 shows the high-temperature part of such a gasoline based fuel cell system developed by *DaimlerChrysler* [2]. In this reforming unit the ATR is thermally coupled with a

Abbreviations: ATR, autothermal reforming/reformer; E-Cat, electrically heatable metallic monolith; HE, heat exchanger; HTS, high-temperature-shift-reactor; POX, partial oxidation; TOX, total oxidation

* Corresponding author. Tel.: +49-711-6493544.
E-mail address: steffen.springmann@web.de (S. Springmann).

0378-7753/$ – see front matter © 2003 Elsevier B.V. All rights reserved.
doi:10.1016/j.jpowsour.2003.09.038

Nomenclature

a_v	specific surface area (m^2/m^3)
c_p	specific heat capacity (kJ/(kmol K))
d	diameter (m)
d_h	hydraulic diameter (m)
D_{eff}	effective dispersion coefficient (kg/(m s))
h	specific enthalpy (kJ/kmol)
Δh_R	reaction enthalpy (kJ/kmol)
l	length (m)
$\dot{m}$	mass flow (kg/(m^2 s))
$\tilde{M}$	molar mass (kg/kmol)
p	pressure (bar)
P	power (kW)
$\dot{q}$	heat flux (kW/m^2)
r	reaction rate (kmol/(m^2 s))
Re	Reynolds number
t	time coordinate (s)
T	temperature (K)
v	gas space velocity (m/s)
$\dot{V}_L$	air flux (m^3/s)
w	mass fraction
z	space coordinate (m)

Greek letters

α	heat transfer coefficient (kW/(m^2 s))
β	mass transfer coefficient (m/s)
δ	Kronecker symbol ($\delta = 1$ for $w^s > w^g$, $\delta = 0$ for $w^s < w^g$)
ϵ	void fraction (m^3/m^3)
ϵ^{st}	emission coefficient
λ	air/fuel-ratio
λ_{eff}	effective heat dispersion coefficient (kW/(m K))
λ	heat conductivity (kW/(m K))
ν	stoichometric coefficient
ρ	density $(kg/m)^3$
σ	emission constant (kW/(m^2 T^4))

Indices

el	electrical
g	gas-phase
heat	electrical heating
i	reaction number
in	inlet
j	component
k	channel number
max	maximum
o	surrounding
out	outlet/exit
s	solid-phase (catalyst-phase)
th	thermal
+	inlet

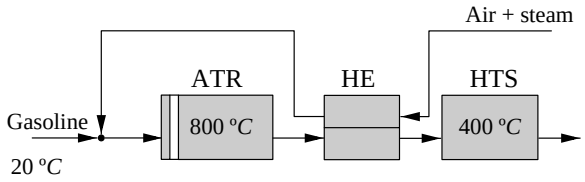

Fig. 1. Sketch of the reforming unit.

high-temperature-shift-reactor (HTS) through a countercurrent heat exchanger.

The feed streams of air and steam are heated up from 200 °C to approximately 600 °C in the heat exchanger. After the injection of liquid gasoline, the feed stream is directed to the ATR, where gasoline is converted autothermally. After the reformat is cooled down to about 400 °C, the CO-content is reduced in the HTS. In the ATR the exothermic partial oxidation of the fuel with air (Eq. (1) + Eq. (2)) is combined with the strongly endothermic steam reforming reaction (Eq. (3)).

$$C_nH_m + \tfrac{1}{2}nO_2 \rightarrow nCO + \tfrac{1}{2}mH_2 \quad (1)$$

$$C_nH_m + (n + \tfrac{1}{4}m)O_2 \rightarrow nCO_2 + \tfrac{1}{2}mH_2O \quad (2)$$

$$C_nH_m + nH_2O \rightarrow nCO + (n + \tfrac{1}{2}m)H_2 \quad (3)$$

By proper adjustment of the air/fuel-ratio λ and the excess of steam H_2O/C, the complete conversion is slightly exothermic and a simple adiabatic reactor set-up can be used. Besides the reforming reactions, two equilibrium limited reactions, the watergas-shift (Eq. (4)) and the methanation reaction (Eq. (5)), must be taken into account.

$$CO + H_2O \rightleftharpoons CO_2 + H_2 \quad (4)$$

$$CO + 3H_2 \rightleftharpoons CH_4 + H_2O \quad (5)$$

Since both reactions are exothermic, CO_2 and CH_4-formation are thermodynamically favoured at low temperatures. Whereas the content of H_2 is increased by the watergas-shift reaction, the methanation reaction results in a loss of H_2. To suppress CH_4-formation in the ATR exit temperatures below 750 °C must be prevented. Under typical operation conditions with air/fuel-ratios of about $\lambda = 0.24$–0.28 and a slight excess of steam ($H_2O/C \approx 2$) H_2-concentrations of about 32% and CO-concentrations of 10% are reached. To increase CO-conversion by the watergas-shift reaction, the HTS is operated at lower temperatures (400–450 °C). Methanation is strongly inhibited by an appropriate shift-catalyst. Thus CO can be reduced to about 4% in the adiabatically operated HTS.

In the concept of *DaimlerChrysler* (Fig. 1) both ATR and HTS are designed as adiabatic, metallic monolith reactors, which are coated with different noble metal catalysts for reforming and watergas-shift reaction. The ATR consists of two monoliths. The first monolith is electrically heatable (E-Cat, 400 cpsi), which is necessary to reach the ignition temperature of the oxidation reactions at the beginning of the

cold start. For the back part of the ATR and the HTS monoliths with 1600 cpsi are used. The heat exchanger is designed as a countercurrent pipe-bundle heat exchanger. Geometric parameters of the ATR, the heat exchanger and the HTS and other model parameters are displayed in Appendix A. The set-up corresponds to reforming units studied by *Daimler-Chrysler* for a thermal load of 33 kW, based on the lower heating value of the gasoline [2]. Both ATR and reforming unit are operated at an inlet pressure of 4 bar.

The model systems for the ATR and the whole reforming unit consist of one-dimensional, dynamic multiphase models. Gas- and solid-phases (catalyst-phases) are balanced separately and are connected by lateral exchange of mass and heat. The model equations, the corresponding boundary conditions and the major model assumptions are given in Appendix B. The reaction kinetics for autothermal reforming and shift-reaction were derived from own experimental results with a new isothermal kinetic reactor [6]. The model systems of partial parabolic differential equations, have been solved with the simulation tool PDEX-Pack developed with the Conrad-Zuse Zentrum, Berlin [7,8].

2. Steady-state operation of the ATR and the reforming unit

Steady-state simulations for the two systems are presented here to simplify the discussion and the assessment of cold start strategies in the following sections. Simulation results for both the ATR and the reforming unit under typical operation conditions are shown in Figs. 2 and 3. In accordance with experimental results the fast exothermic oxidation reactions result in a distinct temperature maximum of the solid/catalyst-phase at the inlet of the ATR (Fig. 2). The subsequent decrease of the temperature can be attributed to the endothermic steam reforming reactions and heat losses. The temperature of the gas-phase approaches the solid-phase temperature by heat transfer within the first

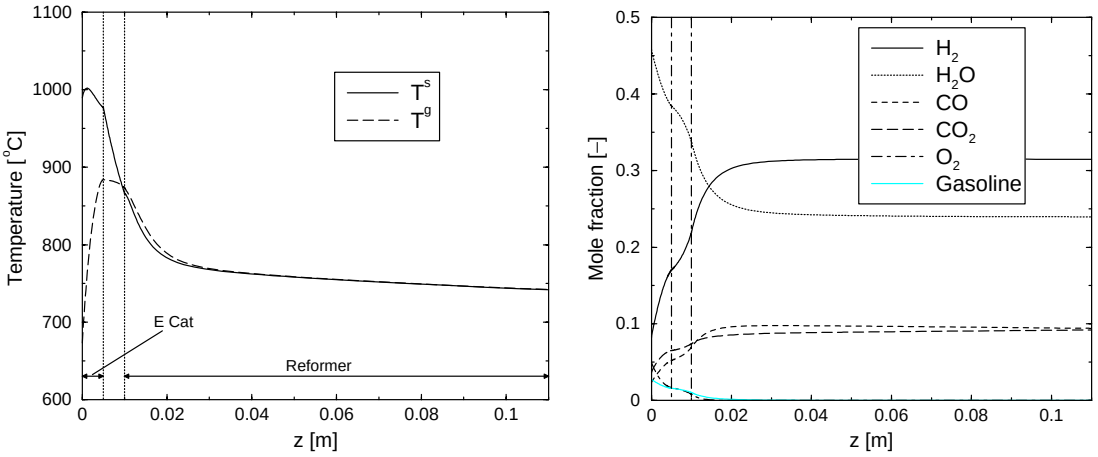

Fig. 2. Temperature and concentration profiles in the ATR; $P_{th} = 33\,kW$, $\lambda = 0.24$, $H_2O/C = 2$, $T^+ = 500\,°C$.

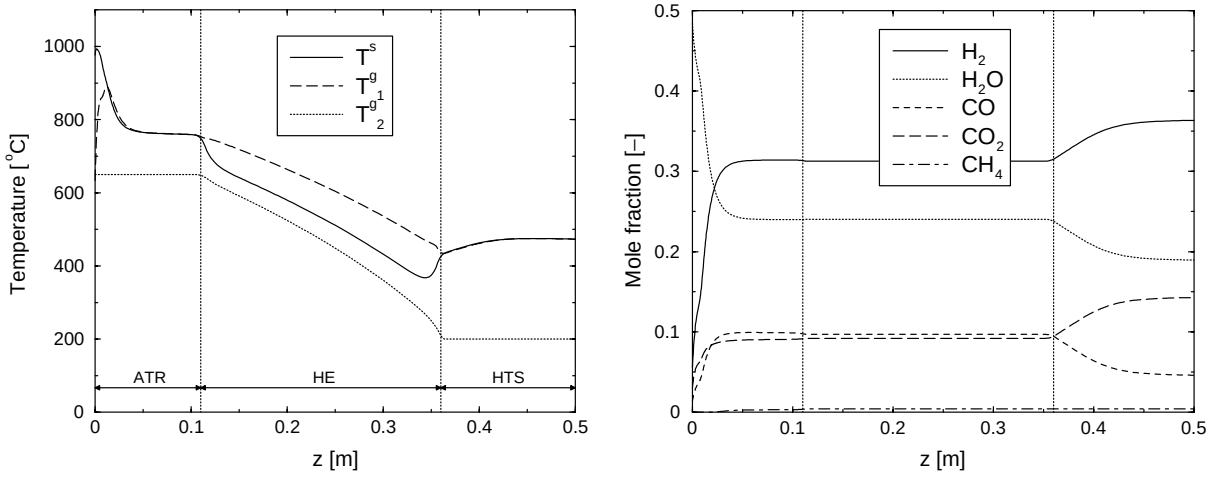

Fig. 3. Temperature and concentration profiles in the reforming unit; $P_{th} = 33\,kW$, $\lambda = 0.24$, $H_2O/C = 2$, $T_1^+ = 20\,°C$, $T_2^+ = 200\,°C$.

two cm of the ATR and the reformat reaches 740 °C at the exit of the ATR. Gasoline and oxygen are fully converted and thus the reformat composition is determined by the equilibrium limited reactions. H_2-concentration at the exit of the ATR is 31.5%. CO-concentration reaches 9.4%, while CH_4 is formed to 0.49%.

Since a countercurrent heat exchanger is used, two gas-phases and one solid-phase (for the catalyst or the separating wall) must be taken into account for the reforming unit (Fig. 3).

The feed stream of air and steam (index 2), flowing from the right to the left side of the heat exchanger, is heated up from 200 °C to about 650 °C. After the injection and evaporation of gasoline, the feed stream is directed to the ATR. The temperature profiles in the ATR for the solid-phase and the gas-phase of the reformat (index 1) are similar to the ATR simulations already discussed. After the ATR, the reformat is cooled down in the heat exchanger to 430 °C at the inlet of the HTS. It is obvious that the heat exchanger design has a major impact on the steady-state and dynamic behaviour of the reforming unit. Due to the exothermic shift reaction the temperature increases again in the HTS. The CO-content is reduced from 9.8 to 4.6% in the shift reactor, while H_2 reaches 36.4%. The simulation results show sufficient good operation of both the ATR and the reforming unit under steady-state operation conditions.

3. Cold start of the ATR

Since the ATR is the first reactor in the whole gas-processing system and is operated at high temperatures, the cold start of the system begins with the heat-up of the ATR to operation temperature. Thus first the start-up behaviour of the ATR alone is discussed in this section.

During cold start several conditions like the ignition temperature of the oxidation reactions on the catalyst and the availability of steam must be taken into account. Therefore, a cold start strategy for the ATR consists of at least three different steps. In the first step the E-Cat is heated up electrically until the catalyst temperature reaches the ignition temperature for the catalytic oxidation (≈400 °C). In the next step the reactive heat-up of the ATR by partial or total oxidation without steam starts (step 2). When steam is available after 60 s the ATR is operated autothermally in step 3.

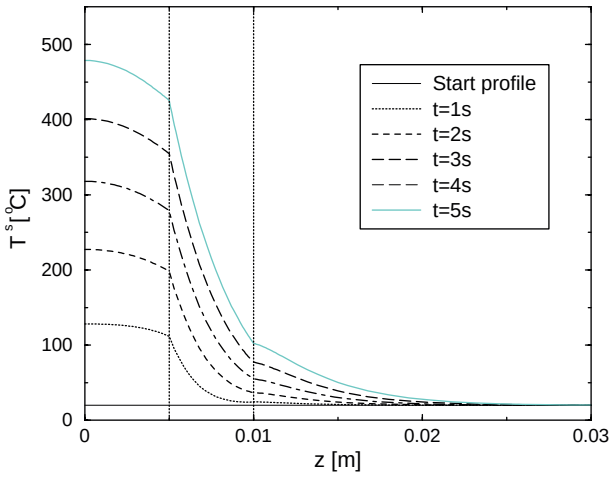

Fig. 4. Temperature profiles of the solid-phase of the ATR during electrical heat-up (step 1); $P_{el} = 2.5$ kW.

Temperature profiles of the solid-phase (catalyst-phase) during electrical heat-up in step 1 with $P_{el} = 2.5$ kW are shown in Fig. 4.

As expected the electrical heat-up of the small E-Cat requires only a short time. After about 4–5 s, the ignition temperature of the oxidation reactions is reached on the catalyst. Starting from the temperature profile after 5 s of electrical heat-up (Fig. 4), the oxidation of gasoline with air in step 2 is possible. The reactive heat-up during this step will take place by partial oxidation (POX, $\lambda < 1$) or by total oxidation

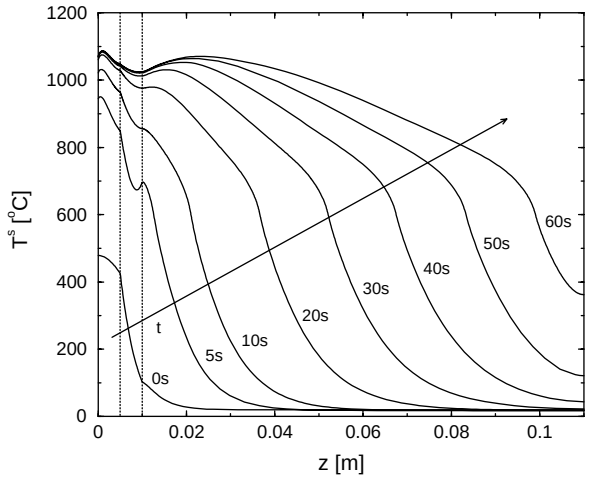

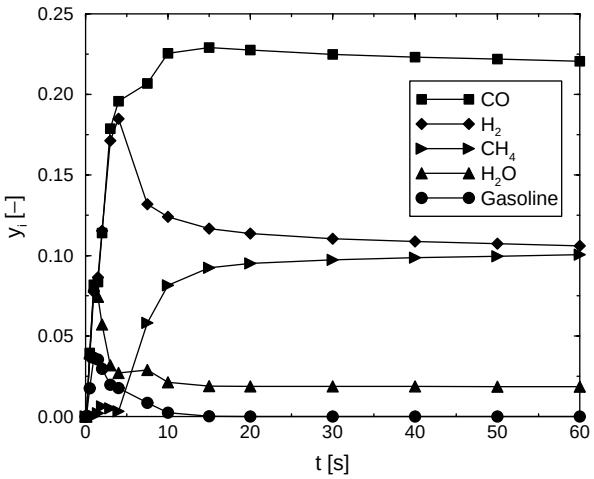

Fig. 5. Temperature profiles over reactor length and ATR exit concentrations over time during step 2 with POX; $P_{th} = 33$ kW, $\lambda = 0.28$, $H_2O/C = 0$, $T^+ = 200$ °C.

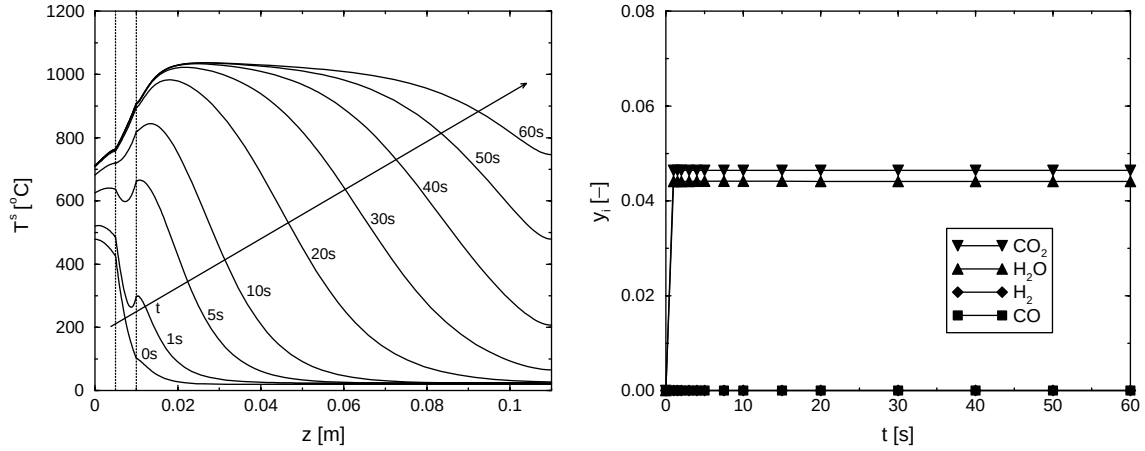

Fig. 6. Temperature profiles over reactor length and ATR exit concentrations over time during step 2 with TOX; $P_{th} = 8\,kW$, $\lambda = 3$, $H_2O/C = 0$, $T^+ = 200\,^\circ C$.

(TOX, $\lambda > 1$), since no steam is available at this time. Fig. 5 displays simulation results for step 2 with POX at full load.

It can be seen, that the ATR is heated up to operation temperature in the front part within this first 60 s. The second temperature peak in the main catalyst is due to CH_4-formation, which is particularly strong since the water content is low. Parameter studies on the partial oxidation during this step indicate, that higher air/fuel-ratios λ result in a faster start-up but also lead to an increase of the maximum temperature in the ATR. The concentration profiles (Fig. 5, right) show full gasoline conversion after 15 s, which is possible, because H_2O is formed during oxidation, which can further convert gasoline via steam reforming. Thus the H_2O-concentration tends to be low, but condensation in the back part of the ATR is possible in the first 45 s. The low content of H_2O also results in significant formation of CH_4 ($y_{CH_4} \approx 10\%$). Although a hydrogen-rich reformat is available after a few seconds with POX, the reformat cannot be used for the fuel cell, since the concentration of CO is too high.

With total oxidation during step 2 the complete heating value of the gasoline is used for the reactive heat-up, as full conversion of gasoline to CO_2 and H_2O is achieved. To avoid too high maximum temperatures a large excess of air with $\lambda = 3$ has been assumed. If heat losses of the ATR are neglected, the maximum temperature in the ATR in this case is independent of the load, but for a high heat release and a fast cold start with TOX, the load should be as high as possible. Due to the high λ, the available load for the cold start is limited by the provided air stream of the compressor. In Fig. 6, simulation results for step 2 with total oxidation are displayed. In this case, the compressor is assumed to operate at its maximum load which results in a thermal load of 8 kW.

As compared to partial oxidation, the temperature increases faster and the ATR is completely heated up to

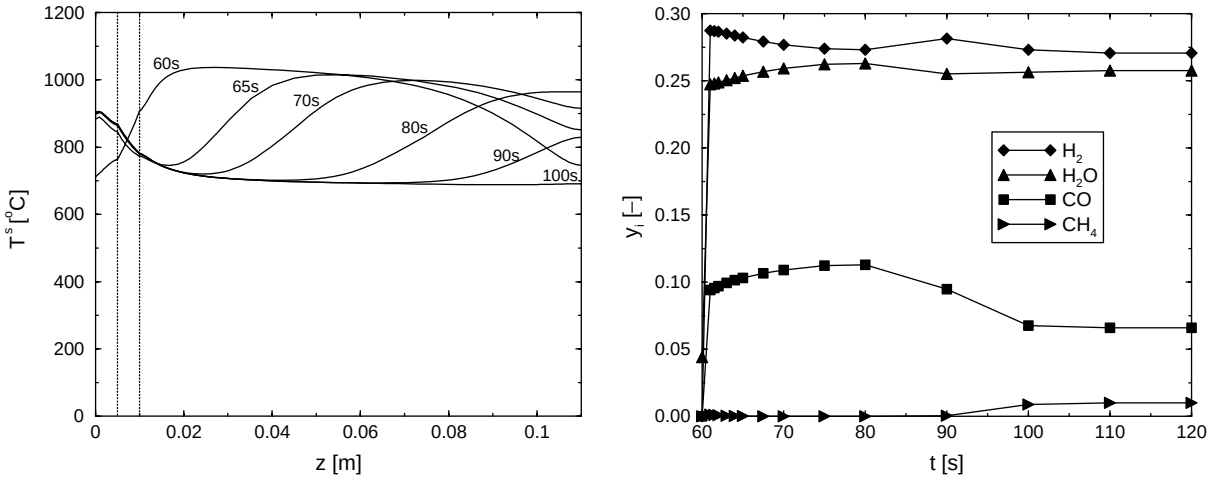

Fig. 7. Temperature profiles over reactor length and ATR exit concentrations over time during step 3; start profile: 60 s with TOX (Fig. 6); $P_{th} = 33\,kW$, $\lambda = 0.28$, $H_2O/C = 2$, $T^+ = 200\,^\circ C$.

operation temperature after 60 s. Due to the large feed stream the temperature maximum in this case is located in the back part of the ATR and not in the E-Cat. Gasoline is fully converted and the only products formed are CO_2 and H_2O. Therefore, the reformat again cannot be used for the fuel cell during this step. Although the H_2O-concentration is lower than with POX during step 2, condensation of steam in the back part of the ATR is possible at the beginning of the cold start.

The simulations show, that in terms of fast and secure start-up of the ATR in the first 60 s without steam, the total oxidation mode is preferred over the partial oxidation mode, provided the large air stream is available. Since the following third step (operation in autothermal mode) is similar for POX and TOX, only the simulation results with TOX in step 2 are presented here (Fig. 7).

Since the ATR is already heated up completely at the beginning of step 3 (60 s), steady-state operation is reached very fast. The concentrations of H_2 and CO increase immediately after the start of water vapour feed, while CH_4 is almost fully converted. Thus right after the addition of steam a proper reformat for the use in subsequent reaction stages is available at the exit of the ATR.

4. Cold start of the reforming unit

Besides the ATR the efficient CO-removal in the HTS is important for the use of the reformat in the fuel cell. As for the ATR the cold start strategy of the reforming unit consists of three different steps. After electrical heat-up of the E-Cat in step 1, the system in operated in partial or total oxidation mode in step 2. When steam is available after 60 s, operation of the system switches to autothermal reforming.

The first step of the cold start of the reforming unit, the electrical heat-up of the ATR, has already been discussed. Fig. 8 shows simulation results of the following steps, step 2 with total oxidation and step 3 with autothermal reforming.

The cold heat exchanger is fed with the ATR exit gas from the left ($z = 0.11$ m) and with the preheated air from the right ($z = 0.36$ m). This causes the depicted temperature profiles in Fig. 8 (left). After about 30 s, the temperature of the air leaving the heat exchanger starts to rise. A short time later the temperature maximum in the ATR becomes critical and either steam must be added or λ must be reduced to prevent catalyst damage by high temperatures. While the ATR again is completely heated up after 60 s, the heat exchanger and the HTS are still cold. Start-up with TOX in step 2 again is slightly faster than with POX. During step 2 with TOX again only CO_2 and H_2O are formed as products. The H_2O-concentration of 5.1% is lower than with POX, but in both cases condensation in the cold parts of the reforming unit is possible. In the right diagram of Fig. 8, the third step beginning with the temperature profile after 60 s with TOX is displayed. It can be seen, that the temperature profile in the ATR falls off within the first 30 s of step 3. This is caused by the addition of steam where only a part of the gasoline is oxidized in the ATR, while the rest is converted via the endothermic steam reforming reactions. Thereby the heat release decreases. After 90 s, a typical temperature profile for autothermal reforming is formed in the ATR. According to the continuously increasing preheat -temperature of the air, the temperature level in the ATR again increases with time. Due to their high heat capacities, the temperature in the heat exchanger and the HTS increases very slowly. Relevant temperatures and exit concentrations for step 3 are shown in Fig. 9.

The drop and subsequent increase of the temperature in the ATR is clearly indicated by the maximum and the exit temperature of the ATR. The inlet temperature of the ATR, as the preheat-temperature of the air/steam stream (not displayed), increases continuously over time. Similarly

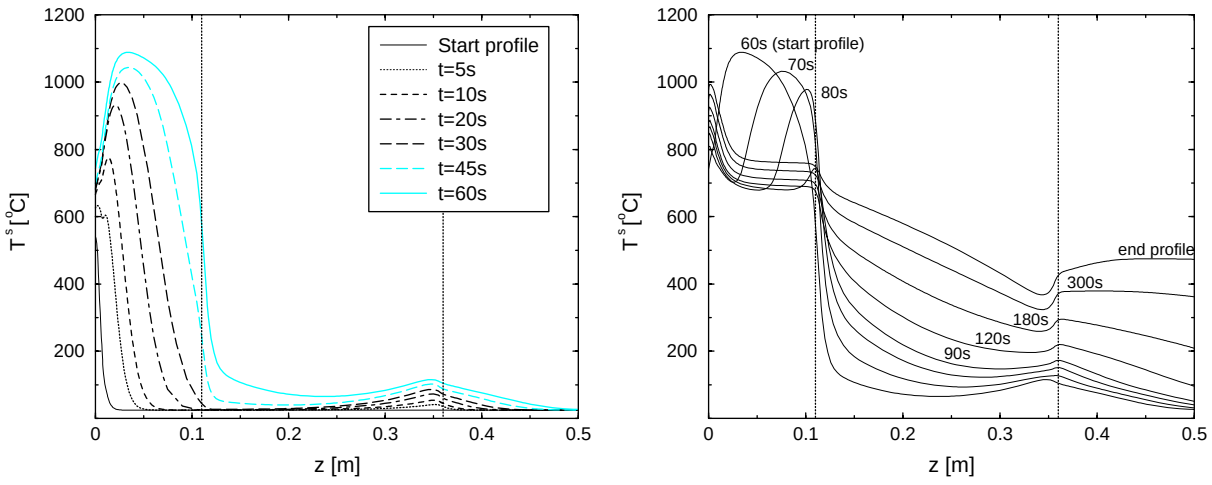

Fig. 8. Temperature profiles during step 2 with TOX (left) and step 3 (right); step 2: $P_{th} = 8$ kW, $\lambda = 2.5$, $H_2O/C = 0$, $T^+_{1/2} = 200/200\,^\circ$C (5–60 s); step 3: $P_{th} = 33$ kW, $\lambda = 0.24$, $H_2O/C = 2$, $T^+_{1/2} = 20/200\,^\circ$C (> 60 s).

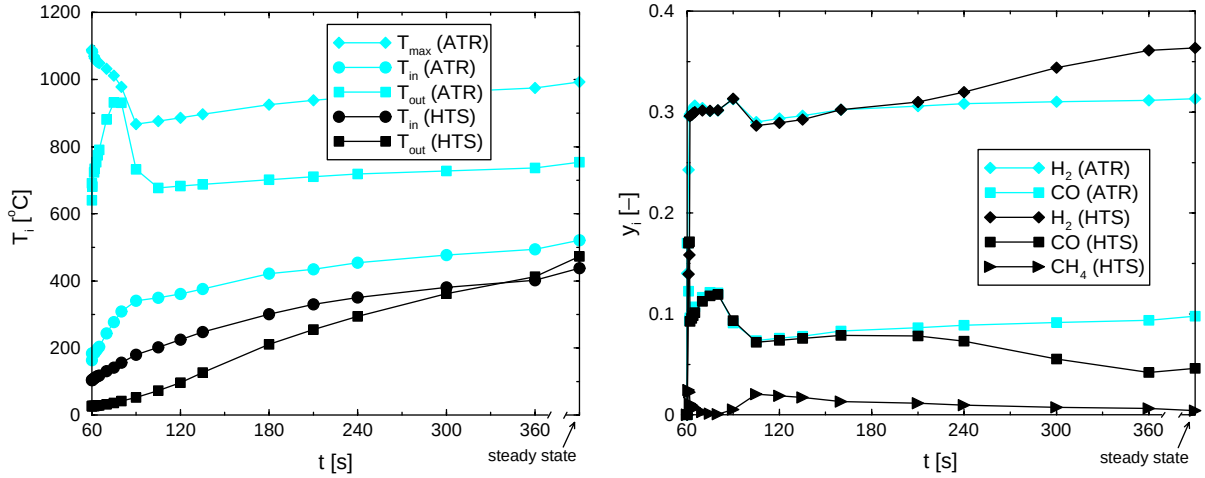

Fig. 9. Temperature and concentration profiles over time during step 3 of the cold start; start profile 60 s with TOX in step 2; $P_{th} = 33$ kW, $\lambda = 0.24$, $H_2O/C = 2$, $T^{+}_{1/2} = 20/200\,^{\circ}C$.

both inlet and exit temperatures of the HTS increase. The addition of steam at 60 s results in the immediate formation of CO and H_2 as indicated by the concentration profiles. The H_2-concentration reaches 30% very fast, while CO in formed to about 10%. All concentrations displayed show the overshoot of the ATR exit temperature during the first 30 s of step 3. The ATR provides a proper reformat with full gasoline conversion and acceptable CO- and H_2-concentrations already after 90 s of the cold start. But at this time, the HTS is still too cold for significant conversion of CO and the concentrations at the exit of ATR and HTS do not differ strongly. The conversion of CO in the HTS starts after about three minutes and after five minutes the CO-concentration drops below 6%. Steady-state operation conditions are reached not before six minutes.

In summary, the cold start of the reforming unit during the first minute in step 2 is dominated by the characteristics of the ATR and the operation with TOX is preferable to POX. During step 3 the ATR has almost reached steady-state operation conditions and the heat capacity of the rest of the reforming unit limits the CO-conversion in the HTS.

5. Measures for cold start acceleration

For a given apparatus design and mass an acceleration of the cold start is only possible by an increase of the heat input into the system. Thereby special attention must be given to the fast start-up of the HTS, as the low CO-conversion limits the cold start of the reforming unit. One option to reduce the start-up time is a simple λ-control during step 3 as displayed in Fig. 10. Since the temperature profile in the ATR drops in the first 30 s of step 3, an operation at higher λ than 0.24 is possible at this time. This results in a higher heat input into the system and should thereby speed-up the cold start.

The maximum temperature in the ATR limts the increase of λ in step 3. As soon as the maximum temperature of the catalyst in reached, λ must be reduced. In this case, the simulation starts with the temperature profile at 60 s with POX or TOX during step 2. After that the reforming unit is operated with $\lambda = 0.3$ between 60 and 150 s and then λ is reduced to 0.24. The simulation results for different cold start strategies including this λ-control in step 3 are shown in Fig. 11. The basic behaviour of all options is similar.

The exit temperature of the ATR drops due to the addition of steam at the beginning of step 3 (60 s) but increases much faster subsequently if λ is increased. Since now the exit temperature of the ATR does not fall below 700 °C, CH_4-formation is effectively suppressed (not displayed). After 150 s, the maximum temperature in the ATR becomes critical (not displayed) and λ is reduced to the value of normal operation conditions. After that steady-state operation in the ATR is reached fast, while the heat-up of the HTS again is very slow.

A reasonable amount of H_2 is already formed in step 3, but the use of the reformat is restricted by its high CO-concentration. Therefore, the different cold start strategies should be compared with respect to their CO-concentrations (Fig. 11, right). The simulation results again confirm, that TOX is preferred to POX during step 2. Moreover, the use of the λ-control strategy results in a

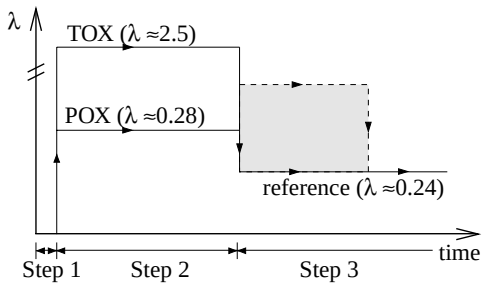

Fig. 10. Influence of λ during step 3 of the cold start (—) without λ-increase, (- - -) with λ-increase.

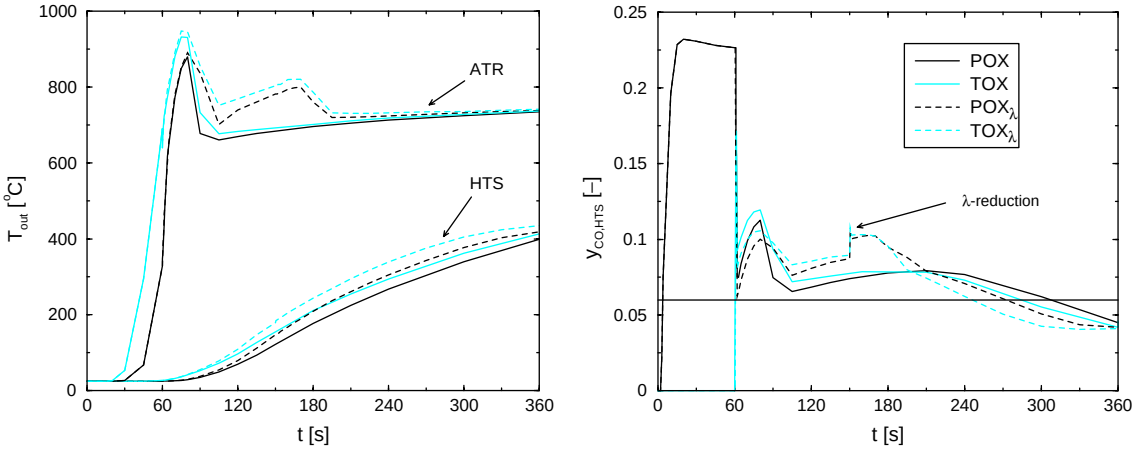

Fig. 11. Temperature and CO-concentration profiles at the exit over time for different cold start strategies; index λ refers to the λ increase during step 3, shown in Fig. 10.

reduction of the start-up time of more than 40 s. After about 4 min, a reformat with acceptable CO-concentration (≈6%) can be provided. A continuous control of λ during step 3 promises a further reduction of the start-up time.

The second measure for the speed-up of the cold start, investigated in this work, is the reactive heat-up of the HTS. Thereby the reformat is partly oxidized with injected air in the HTS. This results in heat generation directly on the catalyst of the HTS. Since the HTS is heated up faster, CO-conversion via the shift-reaction starts earlier. Ignition of CO and H_2 on the catalyst is expected to take place above 200 °C, because of the high CO-content in the reformat. The injected oxygen is fully converted and the oxidation reactions are assumed to be mass transfer limited. After operation with TOX in step 2 in the first 60 s, the system is operated autothermally at higher λ as described above. At 105 s, when the ignition temperature of 200 °C at the inlet of the HTS is reached, the injection of air ($\dot{V}_L = 20$ l/min) and the reactive heat-up starts. At 150 s λ is reduced to normal operation conditions and at 180 s the injection of air into the HTS stops again. On the left side of Fig. 12 temperature profiles at the inlet of the HTS during reactive heat-up with injected air are presented.

It can be seen, that the oxidation of the reformat in the HTS results in a fast increase of the temperature in the HTS. On the right side of Fig. 12 the concentrations of CO and H_2 at the exit of ATR and HTS are displayed over time. As expected the concentrations of both substances in the HTS drop directly at the beginning of the reactive heat-up due to the oxidation reactions (105 s). With the reduction of λ (150 s) and the stop of the air-injection (180 s) the H_2-concentration jumps up and reaches almost steady-state operation conditions. The concentration of CO is slightly increased at 150 s too, but is reduced subsequently via the shift-reaction. The end of the air-injection at 180 s has only a small effect on the CO-concentration.

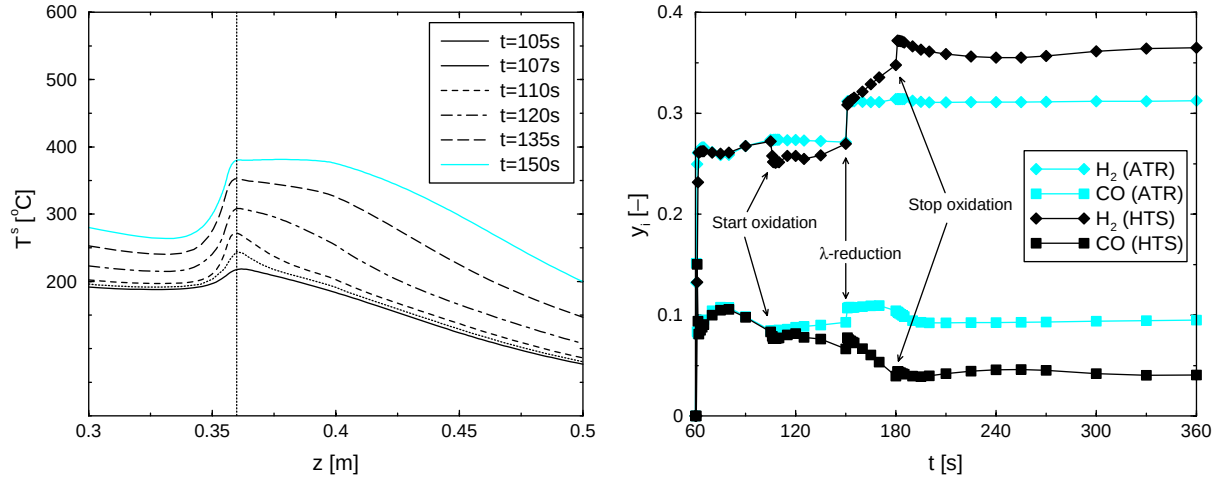

Fig. 12. Temperature profiles at the inlet of the HTS and concentration profiles over time with reactive heat-up in the HTS; step 2 (0–60 s): $P_{th} = 8$ kW, $\lambda = 2.5$, $H_2O/C = 0$, $T^+_{1/2} = 200/200$ °C; step 3 (60–150 s): $P_{th} = 33$ kW, $\lambda = 0.3$, $H_2O/C = 2$, $T^+_{1/2} = 20/200$ °C (>150 s): $P_{th} = 33$ kW, $\lambda = 0.24$, $H_2O/C = 2$, $T^+_{1/2} = 20/200$ °C; air-injection (105–180 s): $\dot{V}_L = 20$ l/min.

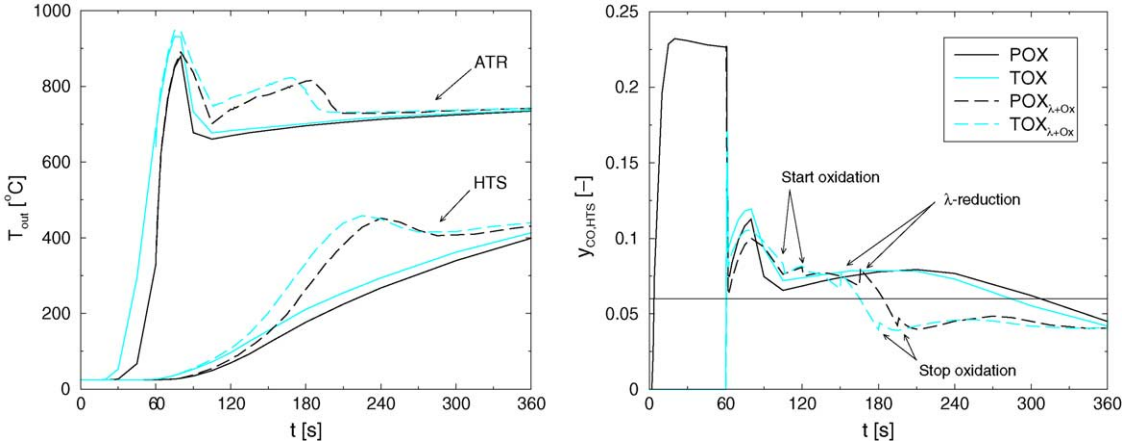

Fig. 13. Temperature and CO-concentration profiles at the exit over time for different cold start strategies; index $\lambda + \mathrm{Ox}$ refers to λ increase and reactive heat-up in the HTS during step 3.

In Fig. 13, temperatures and CO-concentrations at the exit of the ATR and the HTS are presented for different cold start strategies. For both POX and TOX in step 2 the reactive heat-up in the HTS with air reduces the cold start time significantly. With TOX during step 2 the CO-concentration already drops below 6% after 165 s.

As can be expected, higher amounts of air injected result in a faster temperature increase and an earlier conversion of CO in the HTS (Fig. 14). Moreover, the concentrations of CO and H_2 are further reduced by the oxidation with air. The air-injection for the reactive heat-up the HTS is mainly limited by the maximum operation temperature of the shift-catalyst. With an air stream of $\dot{V} = 60$ l/min catalyst damage by high temperatures can still be prevented and the CO-concentration drops below 6% after 115 s.

Due to the high content of CO, the use of the reactive heat-up in the HTS is only possible above the ignition temperature of about 200 °C, which is reached not before 100 s. A further reduction of the start-up time can only be expected, if the ignition temperature of the catalyst can be lowered or the heat-up of the HTS to the ignition temperature can be speeded up. The later can be realized by an electrical heat-up of the HTS, similar to the ignition of the ATR. Therefore, the HTS was divided into two monoliths, of which the first one is elctrically heatable and very short ($l = 5$ mm). An electric power of 2.5 kW again is sufficient for the heat-up of this E-Cat within a few seconds. Under this conditions it is necessary to start the ATR in step 2 in the partial oxidation mode, in order to provide a fuel which can be burned in the HTS. Fig. 15 shows simulation results with this strategy. The reformat formed in the ATR in the first seconds after electrical heat-up, can be ignited on the pre-heated catalyst of the HTS. This results in a rapid temperature increase at the inlet of the HTS already in the first 60 s.

The CO-concentration in the HTS drops due to oxidation and shift-reaction, but still remains too high for the subse-

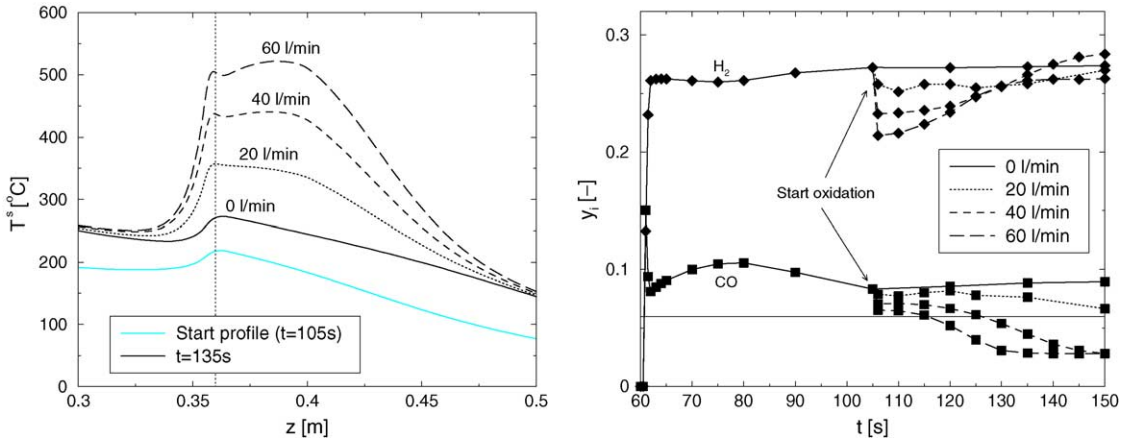

Fig. 14. Temperature profiles along the HTS at 105 s (start of reactive heat-up) and 135 s and exit concentrations over time for different air streams; step 2 (0–60 s): $P_{\mathrm{th}} = 8$ kW, $\lambda = 2.5$, $H_2O/C = 0$, $T^{+}_{1/2} = 200/200$ °C; step 3 (>60 s): $P_{\mathrm{th}} = 33$ kW, $\lambda = 0.3$, $H_2O/C = 2$, $T^{+}_{1/2} = 20/200$ °C.

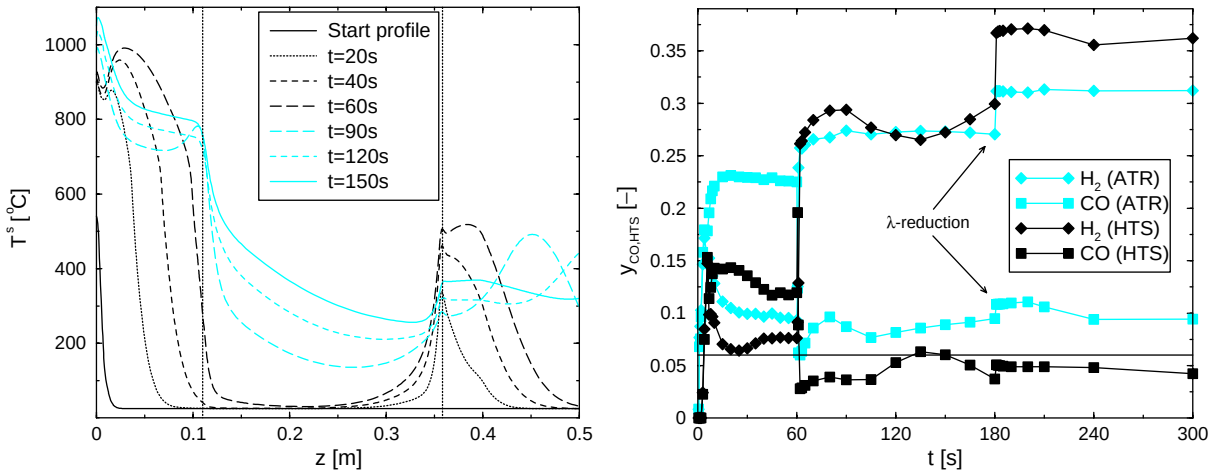

Fig. 15. Temperature profiles and concentrations at the exit over time with reactive heat-up in step 2; $P_{th} = 33\,kW$, $T^{+}_{1/2} = 20/200\,^{\circ}C$; step 2 (0–60 s): $\lambda = 0.3$, $H_2O/C = 0$, $\dot{V}_L = 60\,l/min$; step 3 (60–180 s): $\lambda = 0.3$, $H_2O/C = 2$, $\dot{V}_L = 20\,l/min$ (>180 s): $\lambda = 0.24$, $H_2O/C = 2$, $\dot{V}_L = 0\,l/min$.

quent use. After 60 s, steam is added and the reforming unit is operated autothermally. An increase of λ and a further small injection of air into the HTS prevent strong drops of the temperature profiles in the two reactors (60–180 s). Due to the autothermal operation the concentrations of CO and CH_4 drop immediately and the H_2 content increases. Since the front part of the HTS at this time has already reached operation temperature, CO can be converted sufficiently via the shift-reaction. Thus the HTS exit concentration of CO drops below 6% right after the addition of steam at 60 s, while H_2-concentration reaches about 27%. If necessary the temporary increase of the CO-concentration at the exit of the HTS (t = 110–160 s) can be prevented by a small increase of the air injected during this period.

6. Summary and outlook

The results presented show how the dynamic simulation of the ATR and the reforming unit can support the development of a fast and efficient cold start strategy for gasoline reformers. Different strategies and measures could easily be investigated and assessed. The simulations indicate the electrically supported reactive heat-up of the HTS as the most promising measure for a further reduction of the cold start time. Moreover, the control of λ and the availability of steam during the cold start are of great importance. By optimisation of these measures cold start times for the reforming unit of about 30 s seem to be possible in the future.

Acknowledgements

Support of this work through the DaimlerChrysler AG (Research and Technology, Fuel Cell Systems, Ulm, Germany) and a grant of the German Bundesministerium für Bildung und Forschung (BMBF) is gratefully acknowledged.

Appendix A. Model parameters

Geometric parameters of ATR, heat exchanger and HTS

Parameter	ATR			Heat exchanger	HTS
	E-Cat	Air gap	Reformer		
d (m)	0.07	0.07	0.07	0.1/0.1	0.07
l (m)	0.005	0.005	0.1	0.25	0.14
ϵ^g	0.7	0.95	0.7	0.32/0.46	0.7
a_v (m^2/m^3)	3500	73	6000	256/346	6000

The model parameters for the catalyst-phase correspond to metallic monoliths and are assumed to be constant. The solid-phase density is $\rho^s = 7900\,kg/m^3$, the heat capacity $c^s_p = 0.49\,kJ/(kg\,K)$ and the axial heat conductivity $\lambda^s = 12\,W/(m\,K)$. The gas-phase is assumed to be ideal. Thermodynamic parameters ($c_{p,j}$, h_j) are calculated for every gas component temperature dependent. The transport coefficients for axial dispersion are assumed to be constant: $D^g_{eff} = 0.005\,kg/(m\,s)$, $\lambda^g_{eff} = 5\,W/(m\,K)$.

The transport coefficient α_k for convective heat transfer between gas- and catalyst-phase is $220\,W/(m^2\,K)$ within the monolith structures (ATR, HTS) and $70\,W/(m^2\,K)$ in the heat exchanger. Heat losses of the system were fitted to experimental data of *DaimlerChrysler* for insulated metallic monoliths. The calculated transport coefficients for mass transfer between gas- and catalyst-phase at operation conditions are given below for every component.

Transport coefficients for gas/solid mass transfer

	N_2	CH_4	O_2	H_2O	CO	H_2	CO_2	C_nH_m
β (m/s)	0.1105	0.1173	0.1105	0.1406	0.1093	0.4039	0.0875	0.04

Appendix B. Model assumptions and equations

The models developed consist of one mass-balance for each phase and component, two energy balances for the gas-phases, one for the catalyst/wall-phase and two pressure drop relations for the gas-phases. Since heat conduction of the solid phase (catalyst and wall) is very high, it is assumed, that both catalyst/wall-phases have the same temperature. Channel 2 is only effective in the heat exchanger where catalytic reactions are neglected. The catalytic reactors (ATR, HTS) only consist of channel 1. Thus the state variables of channel 2 are constant in the ATR and the HTS.

The model equations and the corresponding boundary conditions are given below (index k for channel number).

B.1. Mass balances for gas-phases ($k = 1, 2$)

$$0 = \underbrace{-\dot{m}_k \frac{\partial w^{\mathrm{g}}_{j,k}}{\partial z}}_{\text{convection}} + \underbrace{\epsilon^{\mathrm{g}}_k D^{\mathrm{g}}_{\mathrm{eff}} \frac{\partial^2 w^{\mathrm{g}}_{j,k}}{\partial z^2}}_{\text{dispersion}} + \underbrace{a_{v,k}\rho^{\mathrm{g}}_k \beta_j (w^{\mathrm{s}}_{j,k} - w^{\mathrm{g}}_{j,k})}_{\text{mass transfer}} \tag{B.1}$$

The boundary conditions for channel 1 are (channel 2 analogous)

$$\dot{m}_1 w^{g,z=0}_{j,1} - \epsilon^{\mathrm{g}}_1 D^{\mathrm{g}}_{\mathrm{eff}} \left.\frac{\partial w^{\mathrm{g}}_{j,1}}{\partial z}\right|_{z=0} = \dot{m}_1 w^{g,+}_{j,1},$$

$$\left.\frac{\partial w^{\mathrm{g}}_{j,1}}{\partial z}\right|_{z=l} = 0. \tag{B.2}$$

B.2. Mass balances for catalyst-phase ($k = 1$)

$$0 = a_{v,k}\left[\underbrace{\rho^{\mathrm{g}}_k \beta_j (w^{\mathrm{s}}_{j,k} - w^{\mathrm{g}}_{j,k})}_{\text{mass transfer}} - \underbrace{\tilde{M}_j \sum_{i=1}^{I} (r_{i,k}\nu_{ij})}_{\text{reaction}}\right] \tag{B.3}$$

B.3. Energy balances for gas-phases ($k = 1, 2$)

$$0 = \underbrace{-\dot{m}_k c^{\mathrm{g}}_{p,k} \frac{\partial T^{\mathrm{g}}_k}{\partial z}}_{\text{convection}} + \underbrace{\epsilon^{\mathrm{g}}_k \lambda^{\mathrm{g}}_{\mathrm{eff}} \frac{\partial^2 T^{\mathrm{g}}_k}{\partial z^2}}_{\text{dispersion}} + \underbrace{a_{v,k}\alpha_k (T^{\mathrm{s}} - T^{\mathrm{g}}_k)}_{\text{heat transfer}}$$
$$+ \underbrace{a_{v,k} \sum_{j=1}^{J} [\delta_j \rho^{\mathrm{g}}_k \beta_j (w^{\mathrm{s}}_{j,k} - w^{\mathrm{g}}_{j,k})(h_j(T^{\mathrm{s}}) - h_j(T^{\mathrm{g}}_k))]}_{\text{enthalpy transport connected with mass transfer}} \tag{B.4}$$

Boundary conditions for channel 1 are (channel 2 analogous)

$$\dot{m}_1 c^{\mathrm{g}}_{p,1}(T^{g,+}_1 - T^{g,z=0}_1) = -\epsilon^{\mathrm{g}}_1 \lambda^{\mathrm{g}}_{\mathrm{eff}} \left.\frac{\partial T^{\mathrm{g}}_1}{\partial z}\right|_{z=0},$$

$$\left.\frac{\partial T^{\mathrm{g}}_1}{\partial z}\right|_{z=l} = 0. \tag{B.5}$$

B.4. Energy balance for both catalyst/wall phases

$$\underbrace{\rho^{\mathrm{s}} c^{\mathrm{s}}_p \epsilon^{\mathrm{s}} \frac{\partial T^{\mathrm{s}}}{\partial t}}_{\text{capacity}} = \underbrace{\epsilon^{\mathrm{s}} \lambda^{\mathrm{s}} \frac{\partial^2 T^{\mathrm{s}}}{\partial z^2}}_{\text{dispersion}} - \underbrace{a_{\mathrm{o}}\alpha_{\mathrm{o}}(T^{\mathrm{s}} - T^{\mathrm{o}})}_{\text{heat loss}} + \underbrace{\dot{q}_{\mathrm{heat}}}_{\text{elctrical heating}}$$
$$+ \underbrace{\sum_{k=1}^{2}\left[a_{v,k}\sum_{j=1}^{J}[(1-\delta_{j,k})\rho^{\mathrm{g}}_k \beta_j (w^{\mathrm{s}}_{j,k} - w^{\mathrm{g}}_{j,k})(h_j(T^{\mathrm{s}}) - h_j(T^{\mathrm{g}}_k))]\right]}_{\text{enthalpy transport connected with mass transfer}}$$
$$- \underbrace{\sum_{k=1}^{2}[a_{v,k}\alpha_k (T^{\mathrm{s}} - T^{\mathrm{g}}_k)]}_{\text{heat transfer}} - \underbrace{\sum_{k=1}^{2}\left[a_{v,k}\sum_{i=1}^{I}[r_{i,k}\,\Delta h_{R,i,k}]\right]}_{\text{reaction}} \tag{B.6}$$

Boundary conditions are

$$\epsilon^{\mathrm{s}}\lambda^{\mathrm{s}} \left.\frac{\partial T^{\mathrm{s}}}{\partial z}\right|_{z=0} = \underbrace{\epsilon^{\mathrm{st}}\sigma((T^{\mathrm{s}}_{z=0})^4 - (T^{g,+}_1)^4)}_{\text{radiation}}, \quad \left.\frac{\partial T^{\mathrm{s}}}{\partial z}\right|_{z=l} = 0. \tag{B.7}$$

B.5. Pressure drop equations for the gas-phases ($k = 1, 2$)

$$\frac{\partial p_k}{\partial z} = -\frac{64}{Re}\frac{\rho^{\mathrm{g}}_k}{2}\frac{v^2_k}{d_{\mathrm{h}}} \tag{B.8}$$

Boundary condition in this case is a constant feed pressure.

References

[1] J.H.J.S. Thijssen, W.P. Teagan, Long-term prospects for PEMFC and SOFC in vehicle applications, SAE Pap. SP-1691 (2000) 145–158.

[2] PEMTECH, Development of the PEM-technology for mobile applications, Final report no. 03270067, 1998–2002.

[3] Transportation fuel cell power systems, Annual progress report, US Department of Energy, 2000.

[4] M. Fronk, On-board gasoline reforming: the bridge to the hydrogen fuel cell vehicle, in: Proceedings of the 7th Grove Fuel Cell Symposium, 2001.

[5] S.R. Ellis, S.E. Golunski, M.I. Petch, Hotspot processor for reformulated gasoline, Report ETSU F/02/00143/REP, DTI/Pub URN 01/958, Johnson Matthey Technology Center, 2001.
[6] S. Springmann, G. Friedrich, M. Sommer, M. Himmen, G. Eigenberger, Isothermal kinetic measurments for hydrogen production from hydrocarbon fuels using a novel kinetic reactor concept, Appl. Catal. A: Gen. 235 (2002) 101–110.
[7] U. Nowak, J. Frauhammer, U. Nieken, A fully adaptive algorithm for parabolic partial differential equations in one space dimension, Comput. Chem. Eng. 20 (1996) 547–561.
[8] J. Frauhammer, Numerische Loesung von eindimensionalen parabolischen Systemen mit adaptiven Gittern, Master Thesis, ICVT, University Stuttgart, 1992.